Photon-electron polarization correlations in high-Z ns-subshell photoionization

Young Soon Kim
Department of Physics, Myong Ji University, Yong-In 449-728, Korea

I. B. Goldberg
Racah Institute of Physics, Hebrew University of Jerusalem, Jerusalem 91904, Israel

R. H. Pratt
Department of Physics and Astronomy, University of Pittsburgh, Pittsburgh, Pennsylvania 15260
(Received 18 March 1991)

We present a comprehensive survey of the behavior of all correlations C_{ij} between the polarization of the incoming photon and the spin of the outgoing photoelectron, for ejection from all subshells of uranium, for electron energies from 1 eV to 100 keV. The correlations for ns-subshell photoionization are reported here. The numerical results for these polarization correlations are obtained within the independent-particle approximation in a relativistic self-consistent atomic field (Dirac-Slater type), including all significant multipole contributions. We confirm that at low photon energies (up to ~ 1 keV), which means relatively low kinetic energy ε for the photoelectron and ejection from a subshell of high n, dipole predictions are generally valid, reproducing the full numerical results, including the abrupt changes in the shape of the C_{ij} curves as functions of the ejection angle θ. As photon energy increases, the correlation coefficients become complicated functions of θ, losing symmetry around $\theta=90°$. For higher ε, the correlation coefficients of different n tend to merge into a common curve as a function of θ, although the shape of the curve keeps changing as ε increases, as we have previously reported for angular distributions.

PACS number(s): 32.80.Fb

I. INTRODUCTION

We wish to report a theoretical study and comprehensive survey, within the independent-particle approximation, of all possible correlations in photoionization between the polarization of the incoming photon and the spin of the ejected outgoing photoelectron, for all subshells of uranium, for an electron energy range from 1 eV to 100 keV. We begin in this paper by reporting and discussing the correlations in ns-subshell photoionization.

Previously, we studied total cross sections and angular distributions of photoelectrons from high-Z elements numerically in a relativistic self-consistent atomic field (Dirac-Slater type), including all the significant multipole contributions [1,2]. The numerical results presented here for the polarization correlations C_{ij} are obtained through the same relativistic single-particle scheme, based on the characterization given by Pratt and co-workers [1,3–5], as

$$\frac{d\sigma}{d\Omega}(\xi,\zeta)=\left[\frac{d\sigma}{d\Omega}\right]_{\text{unpol}}\left[\frac{1}{2}\sum_{i,j=0}^{3}\xi_i\zeta_j C_{ij}\right], \tag{1}$$

where the photon polarization is described with the Stokes parameters ξ_i and the unit vector ζ specifies the spin direction of the ejected electron in its rest system, with $\xi_0=\zeta_0=C_{00}=1$. Details for the characterization and for the coordinate system are given in Sec. II. We also give in Sec. II the reduction of the full multipole formalism for the C_{ij}, given in Refs. [1] and [3], to a dipole form for ns subshells in the long-wavelength limit.

With advances in photon sources such as lasers and synchrotron radiation, detailed studies directed toward the "complete" description of atomic and molecular photoionization have been receiving much attention lately [6]. It has been known for a long time that photoelectrons are spin polarized in the relativistic region. Fano pointed out in 1969 [7] that the slight difference in energy positions of Cooper minima (the zeros of the radial matrix elements) in $ns\rightarrow\epsilon p_{1/2}$ and $ns\rightarrow\epsilon p_{3/2}$ channels due to the spin-orbit interaction leads to a large spin polarization of the photoelectrons in the visible or uv range, and it is by now well known that spin-polarized electrons may be ejected from unpolarized atoms by photons of any polarization state including unpolarized photons [6].

Theoretical formulations to describe photoelectron spin polarization have been developed by many authors, including Cherepkov [8], who presented the results in the random-phase approximation with exchange, Lee [9] in the multichannel quantum-defect theory applied to the helicity formalism, Klar [10] using the angular-momentum-transfer formalism to include anisotropic electron-ion final-state interactions, and Huang [11] in the relativistic random-phase approximation. These authors have included effects beyond the independent-particle approximation, but the results are specialized to the electric dipole ($E1$) transition. Scofield [12] has recently reported relativistic calculations in independent-particle approximation for the angular distribution of photoelectrons from linearly polarized photons.

As noted in Ref. [3], where C_{ij} for K-shell photoeffect from $Z=13$ to 92 and the range of energies from 220 keV to 2 MeV were studied with all the relativistic multipole contributions included, the photoeffect can serve as a polarizer of electrons, a transmitter of polarization from photons to electrons, or an analyzer of polarized radiation. Hence, the photoionization process can be used as a way to produce polarized electrons with, for example, photons from synchrotron radiation (elliptically polarized vuv photons ranging from linear through circular polarization depending on the direction of emission). The fact that such photon beams are polarized also means the polarization correlations may be needed in order to interpret photoionization experiments. Information as to how the spin of the outgoing photoelectron is correlated to the polarization of the incoming photon is essential.

In the dipole approximation, the photoionization from an $(nL)_J \equiv nK\,[K=(-1)^{J+L+1/2}(J+\frac{1}{2})]$ subshell may be fully specified by five parameters, which are expressed in terms of the five independent dipole quantities: three radial dipole matrix elements and two relative phases. Of course, for $J=\frac{1}{2}$ subshells, only three parameters are independent; they can be written in terms of the two radial matrix elements and the only one relative phase of that case. Experimentally, when this type of dipole description is valid, three of the five parameters may be determined with unpolarized photons: the total cross section σ_{nK} and the asymmetry parameter β_{nK} of angular distribution for the differential cross section

$$\left[\frac{d\sigma_{nK}}{d\Omega}\right]_{\text{unpol}}=\frac{\sigma_{nK}}{4\pi}[1-\tfrac{1}{2}\beta_{nK}P_2(\cos\theta)]\ , \tag{2}$$

averaged over the initial and the final magnetic substates of the atom and the ion, respectively, and averaged over the initial photon polarization and summed over the final electron spin. The third parameter can be taken as the degree of transverse polarization of electrons from unpolarized photons,

$$P_t(\theta)=\frac{N_\uparrow-N_\downarrow}{N_\uparrow+N_\downarrow}\ ,$$

where $N_\uparrow$ and $N_\downarrow$ are the number of electrons with spin up and down along the axis perpendicular to the production plane defined by the two momenta $\mathbf{k}$ and $\mathbf{p}$ of the incoming photon and the ejected photoelectron, respectively, and θ is the angle between the two momenta. Evidently

$$N_\uparrow+N_\downarrow=\left[\frac{d\sigma_{nK}}{d\Omega}\right]_{\text{unpol}}=\frac{\sigma_{nK}}{4\pi}[1-\tfrac{1}{2}\beta_{nK}(\tfrac{3}{2}\cos^2\theta-\tfrac{1}{2})]\ , \tag{3}$$

as given by Eq. (2). Later, in Sec. II, we will see that $P_t(\theta)$ carries the same information as our correlation $C_{02}(\theta)$, which is closely related to the quantity called η by Huang [11], though others prefer a different name (for example, ξ in Refs. [6], [9], and [13].)

Experimental determination of the remaining two of the five dipole parameters involves measurements with circularly polarized photons: transverse polarization of the photoelectron spin in the production plane and the transmission of photon helicity (γ and P_z, respectively, in Ref. [6]), or the longitudinal and the transverse spin polarization in the reaction plane (ζ and ξ in Ref. [11], γ and δ in Refs. [9] and [10]), which are related to our C_{33} and C_{31} of Sec. II, respectively, in the dipole regime. Measurements with linearly polarized photons do not give additional independent information on polarization correlations within the dipole approximation.

When we consider higher multipole contributions, there are four more independent correlations—C_{10}, C_{21}, C_{23}, and C_{12}—observable with linearly polarized photons, and each of the C_{ij} can no longer be represented as a single energy-dependent parameter multiplied by simple trigonometric angular factors as in the dipolar regime. [For angular distributions likewise, we also need in principle infinitely many angular distribution parameters B_k, instead of the single angular distribution parameter β of the dipole limit, as discussed in Refs. [1,2], such that $d\sigma/d\Omega=(\sigma/4\pi)\sum_{k=0}^{\infty}B_kP_k(\cos\theta)$, with $B_0\equiv1$ and $B_2\cong-\frac{1}{2}\beta$ at low photon energies.] Not counting $C_{00}\equiv1$, only these seven correlations among the seemingly possible fifteen C_{ij} are permitted to be nonzero from the invariance consideration given in Refs. [1,3].

Numerical results for the C_{ij} as functions of the angle θ, for various photoelectron kinetic energies ε ranging from 1 eV up to 100 keV, for all the ns subshells of uranium, are shown and discussed in Sec. III.

At low photon energies ($\lesssim1$ keV), i.e., low ε and high n, we find that the C_{ij} may be well described in terms of their dipole reductions, with such typical features as an abrupt change in sign and symmetry in θ of C_{ij} curves near Cooper minima, where one of the two radial matrix elements ($ns\rightarrow\varepsilon p_j; j=\frac{1}{2},\frac{3}{2}$) goes through zero. As ε increases higher multipole contributions beyond dipole (and the retardation effects) begin to be important. At high ε, for each C_{ij} the set of curves for a given K for all n tend to merge into a common curve, for the same reason discussed in Ref. [2] for the merging of the angular distribution coefficients B_k (the C_{ij} and the B_k are determined from the same transition matrix elements). But the shapes of the curves as functions of θ keep changing with energy, as was seen in Ref. [3], since the higher the photon energy, the higher the order of significantly contributing multipoles.

For subshells other than ns, which we will report and discuss in subsequent planned papers in this series, we can also expect to see the effects of shape resonances at intermediate photoelectron energies for higher-L states (as in our earlier study of angular distributions), resulting in additional energy-dependent variations.

II. POLARIZATION CORRELATIONS AND THEIR DIPOLE REDUCTIONS

In this section, we obtain for ns subshells the reduction of the expressions for the C_{ij} given in Ref. [1] into their

dipole forms. As shown in Fig. 1, our coordinate system is centered at the atomic nucleus with the $\hat{\mathbf{z}}$ axis along $\mathbf{k}$, $\hat{\mathbf{y}}$ along $\mathbf{k}\times\mathbf{p}$, and the $\hat{\mathbf{x}}$ axis in the $(\mathbf{k},\mathbf{p})$ plane as in Ref. [1], so that the production plane is the $\hat{\mathbf{x}}-\hat{\mathbf{z}}$ plane. The photon polarization vector $\boldsymbol{\epsilon}=\epsilon_1\hat{\mathbf{x}}+\epsilon_2\hat{\mathbf{y}}$, with $|\epsilon_1|^2+|\epsilon_2|^2=1$, is described with Stokes parameters [6,14] in this coordinate system,

$$\begin{aligned}\xi_1&=\epsilon_1^*\epsilon_1-\epsilon_2^*\epsilon_2\ ,\\ \xi_2&=\epsilon_1\epsilon_2^*+\epsilon_1^*\epsilon_2\ ,\\ \xi_3&=i(\epsilon_1\epsilon_2^*-\epsilon_1^*\epsilon_2)\ ,\end{aligned}\tag{4}$$

or in the compact Jones vector notation [15] for the photon polarization $\langle\boldsymbol{\epsilon}|=[\epsilon_1^*,\epsilon_2^*]$, as

$$\xi_i=\langle\boldsymbol{\epsilon}|\sigma_{i+2\atop i-1}|\boldsymbol{\epsilon}\rangle\ ,\tag{5}$$

with σ_i of the form as the (2×2) Pauli spin matrices. Here, $\xi_1=\pm1$ corresponds to linear polarization along the $\hat{\mathbf{x}}$ and $\hat{\mathbf{y}}$ directions (i.e., in or perpendicular to the production plane), respectively; ξ_2 is a degree of linear polarization along $\phi=45°$($\xi_i=-1$ is the polarization orthogonal to $\xi_i=+1$), ξ_3 represents the degree of circular polarization of photons. Also note that $\boldsymbol{\epsilon}\cdot\mathbf{k}=\epsilon_3=0$, which means that the radiation gauge has been chosen. In this gauge, which is sometimes called the transverse or Coulomb gauge, the relativistic transition matrix elements reduce to the velocity form in the nonrelativistic (NR) dipole limit, which in turn can be expressed in a local potential in terms of the length form.

The spin polarization of the ejected electron is specified by its spin direction $\boldsymbol{\zeta}=\langle\chi|\boldsymbol{\sigma}|\chi\rangle$ in its rest system, with

$$\zeta_1=\boldsymbol{\zeta}\cdot(\hat{\mathbf{y}}\times\hat{\mathbf{p}})\ ,\quad \zeta_2=\boldsymbol{\zeta}\cdot\hat{\mathbf{y}}\ ,\quad \zeta_3=\boldsymbol{\zeta}\cdot\hat{\mathbf{p}}\ .\tag{6}$$

Note that the coordinate axes $(\hat{\mathbf{1}},\hat{\mathbf{2}},\hat{\mathbf{3}})$ for the final-electron state are rotated from the initial axes $(\hat{\mathbf{x}},\hat{\mathbf{y}},\hat{\mathbf{z}})$ by the ejection angle θ around the $\hat{\mathbf{y}}$ axis. Hence, ζ_1 and ζ_2 are the transverse components of the spin of the ejected photoelectron in and perpendicular to the production plane, respectively, in its rest system, and ζ_3 the longitudinal component.

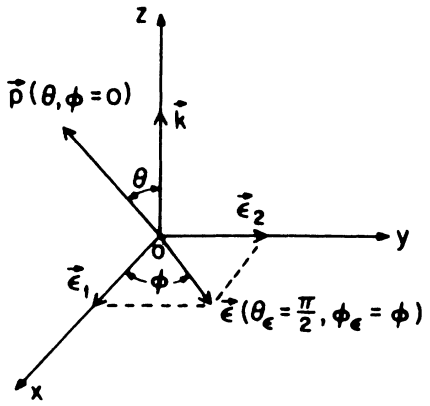

FIG. 1. Coordinate system employed in this work.

Assuming that the polarizations of the initial bound state and the residual ionic state are not observed, the seven nontrivial C_{ij} defined in Eq. (1), other than $C_{00}\equiv1$, are given in Ref. [1] in terms of the transition matrix $A^{\pm}_{\pm}$ with all multipoles included, and the relative phase shifts δ. We will not give the cumbersome details here.

For ns subshells, $L=0$, $K=-(J+\frac{1}{2})=-1$ as $J=\frac{1}{2}$. Taking only the $E1$ contribution we get for the transition from the ns to the $\epsilon p_{1/2}(\kappa=1)$ channel.

$$\begin{aligned}A^{+}_{+}&=0\ ,\quad A^{-}_{+}=\sqrt{\tfrac{2}{3}}Y_{1-1}(\hat{\mathbf{p}})(s_1+\tfrac{1}{3}s_2)\ ,\\ A^{+}_{-}&=0\ ,\quad A^{-}_{-}=-\sqrt{\tfrac{1}{3}}Y_{10}(\hat{\mathbf{p}})(s_1+\tfrac{1}{3}s_2)\ ,\end{aligned}\tag{7}$$

and from the ns to the $\epsilon p_{3/2}(\kappa=-2)$ channel,

$$\begin{aligned}A^{+}_{+}&=\sqrt{\tfrac{2}{3}}Y_{11}(\hat{\mathbf{p}})s_2\ ,\quad A^{-}_{+}=-\sqrt{\tfrac{2}{27}}Y_{1-1}(\hat{\mathbf{p}})s_2\ ,\\ A^{+}_{-}&=0\ ,\quad A^{-}_{-}=-\sqrt{\tfrac{4}{27}}Y_{10}(\hat{\mathbf{p}})s_2\ ,\end{aligned}\tag{8}$$

where

$$\begin{aligned}s_1&=\int_0^\infty dr\, j_0(kr)G_K f_\kappa\ ,\\ s_2&=\int_0^\infty dr\, j_0(kr)g_\kappa F_K\ ,\end{aligned}\tag{9}$$

with $G_K(g_\kappa)$ and $F_K(f_\kappa)$ the large and small components of the Dirac radial wave functions of the bound (continuum) electrons as defined in Ref. [1].

The connection between these radial transition matrix elements and the $E1$ elements is given as follows. The radial matrix elements for the 2^Λ-pole electric transition ($E\Lambda$) may be written in the Coulomb gauge as [12]

$$R^{E\Lambda}=\int dr\left[(-\Delta\kappa)(fG+gF)\left[-j_{\Lambda-1}(kr)+\frac{\Lambda j_\Lambda(kr)}{kr}\right]+\Lambda(\Lambda+1)(fG-gF)\frac{j_\Lambda(kr)}{kr}\right]\tag{10}$$

or

$$\begin{aligned}R^{E\Lambda}=\int dr\{&fG[(\Lambda+1)(\Delta\kappa+\Lambda)j_\Lambda(kr)/kr-\Delta\kappa j_{\Lambda+1}(kr)]\\&+gF[(\Lambda+1)(\Delta\kappa-\Lambda)j_\Lambda(kr)/kr-\Delta\kappa j_{\Lambda+1}(kr)]\}\ ,\end{aligned}\tag{11}$$

using the recursion formula for the spherical Bessel functions, with $\Delta\kappa=\kappa-K$, omitting the subscripts κ and K for simplicity. In the long-wavelength limit, as $kr\to0$, $j_\Lambda(kr)/kr\to j_{\Lambda-1}(kr)/(2\Lambda+1)$ and only the lowest-order term in kr should be kept to be consistent. Then,

$$R^{E\Lambda}\to\frac{\Lambda+1}{2\Lambda+1}\left[(\Delta\kappa+\Lambda)\int Gfj_{\Lambda-1}(kr)dr+(\Delta\kappa-\Lambda)\int gFj_{\Lambda-1}(kr)dr\right]\tag{12}$$

and

$$R^{E1}\to\tfrac{2}{3}[(\Delta\kappa+1)s_1+(\Delta\kappa-1)s_2]\tag{13}$$

to the lowest order in kr. Since $\Delta\kappa=2$ for $ns\to\epsilon p_{1/2}$ and

$\Delta\kappa=-1$ for $ns\rightarrow\varepsilon p_{3/2}$, defining $R^{E1}(ns\rightarrow\varepsilon p_j)\equiv R_j$ and writing $R_{1/2}$ and $R_{3/2}$ as R_1 and R_3, respectively, we get

$$2\left[s_1+\frac{s_2}{3}\right]=R_1\ ,\quad -\tfrac{4}{3}s_2=R_3\ . \tag{14}$$

Substituting these into $A_{\pm}^{\pm}$ and Eq. (5.1.19) of Ref. [3], we obtain the following dipole expressions for ns subshells in the long-wavelength limit:

$$\begin{aligned}D_{00}&=\frac{1}{32\pi}[2(R_1^2+R_3^2-2R_1R_3\cos\delta)\\&\quad+3\sin^2\theta(R_3^2+2R_1R_3\cos\delta)]\\&=\frac{1}{16\pi}[(R_1^2+2R_3^2)\\&\quad-(R_3^2+2R_1R_3\cos\delta)P_2(\cos\theta)]\ ,\end{aligned}\tag{15}$$

$$C_{02}=-3\sin\theta\cos\theta R_1R_3\sin\delta/(16\pi D_{00})\ , \tag{16}$$

$$C_{10}=3\sin^2\theta(R_3^2+2R_1R_3\cos\delta)/(32\pi D_{00})\ , \tag{17}$$

$$C_{12}=C_{02}\ , \tag{18}$$

$$C_{21}=3\sin\theta R_1R_3\sin\delta/(16\pi D_{00})\ , \tag{19}$$

$$C_{23}=0\ , \tag{20}$$

$$C_{31}=\sin\theta(R_1^2-2R_3^2+R_1R_3\cos\delta)/(16\pi D_{00})\ , \tag{21}$$

$$C_{33}=\cos\theta(R_1^2+R_3^2-2R_1R_3\cos\delta)/(16\pi D_{00})\ , \tag{22}$$

where

$$\delta=\delta_1-\delta_3(\equiv\delta_{1/2}-\delta_{3/2})$$

is the difference between the phase shifts of the two channels, and

$$D_{00}=\frac{k}{16\pi pE\alpha}\left[\frac{d\sigma}{d\Omega}\right]_{\text{unpol}}\ .$$

Defining [16]

$$\begin{aligned}&\bar{\sigma}\equiv R_1^2+2R_3^2\ ,\\&\beta\equiv 2(R_3^2+2R_1R_3\cos\delta)/\bar{\sigma}\ ,\\&\eta\equiv 3R_1R_3\sin\delta/\bar{\sigma}\ ,\\&\zeta\equiv(R_1^2+R_3^2-2R_1R_3\cos\delta)/\bar{\sigma}=1-\beta/2\ ,\\&\xi\equiv(R_1^2-2R_3^2+R_1R_3\cos\delta)/\bar{\sigma}\end{aligned}\tag{23}$$

for the five dipole parameters in this limit, the matrix $C=[C_{ij}]$ becomes identical to the matrix Λ divided by $1-\frac{1}{2}\beta P_2(\cos\theta)$, described by Huang in Eq. (5.24) of Ref. [11], except that in our coordinate system $\phi=0$ and that his Stokes parameters S_i are related to our ξ_i as $S_1=-\xi_1$, $S_2=-\xi_2$, and $S_3=\xi_3$, and his matrix elements D_j are given by $D_j=(3/2\pi)C_je^{i\delta_j}R_j$, where

$$C_j=\begin{cases}-\left[\dfrac{(2J-1)(2J+1)}{12J}\right]^{1/2}\ , & j=J-1>0\\[2ex]\left[\dfrac{2J+1}{12J(J+1)}\right]^{1/2}\ , & j=J\\[2ex]\left[\dfrac{(2J+1)(2J+3)}{12(J+1)}\right]^{1/2}\ , & j=J+1\ .\end{cases}$$

[It can be easily seen that only three of the above five parameters in Eq. (23) are independent, though the relationship between ξ and the others does not reduce to a simple form to give further insight.]

III. RESULTS AND DISCUSSION

Figures 2–9 show the calculated results for the seven nontrivial C_{ij} as functions of θ, for all ns subshells of uranium with photoelectron energies from 1 eV to 100

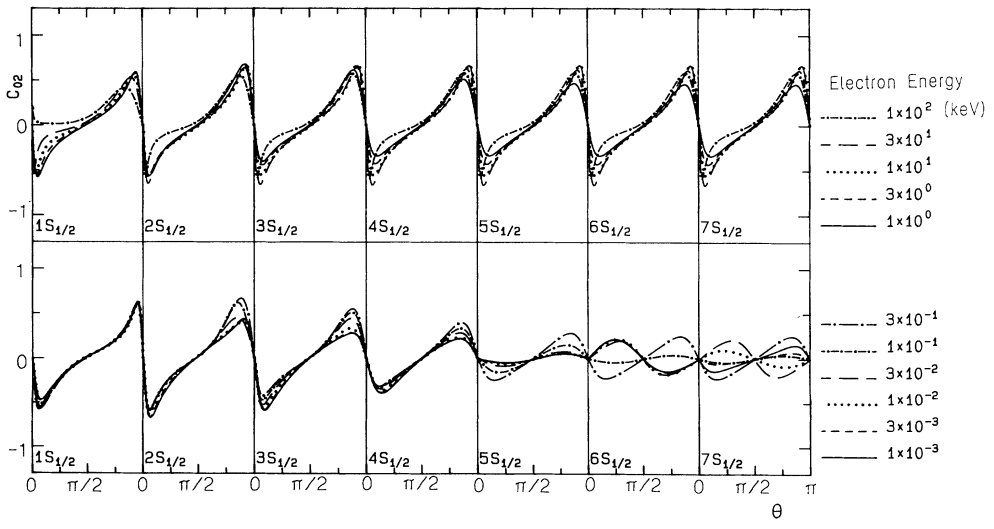

FIG. 2. Numerical results of C_{02} for uranium ns subshells calculated in a Dirac-Slater-type potential including all the significant multipole contributions. Electron kinetic energies are given in keV.

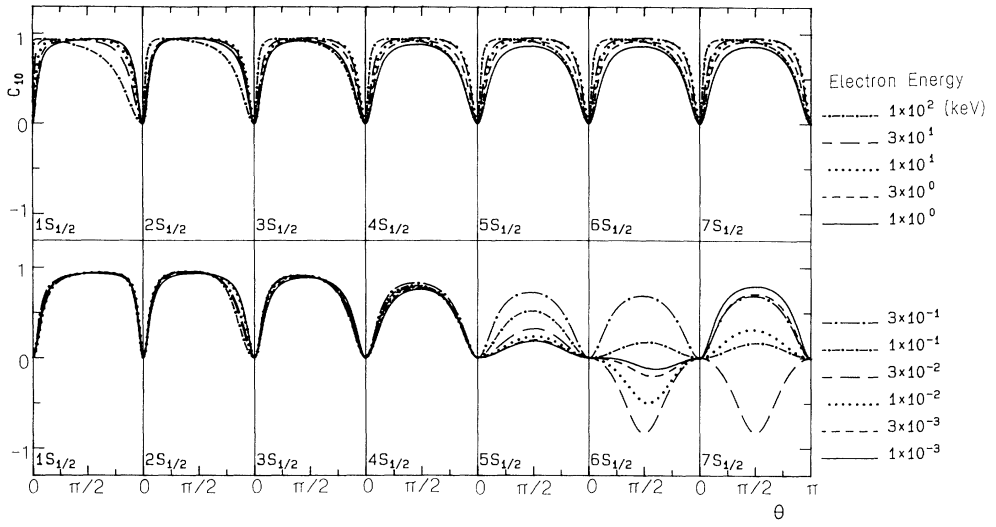

FIG. 3. The same as Fig. 2 for C_{10}.

keV. Figures 2–8 exhibit the variation with energy for each given *ns* state, while Fig. 9 permits the comparison of different *ns* states for six different energies $\varepsilon=10^{-3}$, 10^{-2}, 10^{-1}, 1, 10, and 10^{2} keV. Curves for C_{12} are similar to C_{02} and are omitted in Fig. 9; the similarity held when ε was as high as 208 keV in Ref. [3]. Curves for C_{23} are almost zero and are omitted. Figures 10 and 11 show the dipole predictions and their differences from the full multipole results in the same arrangement as Fig. 9. In the dipole case $C_{23}(=0)$ and $C_{12}(=C_{02})$ are not shown. Figure 12 shows the dipole parameters β, ξ, η, and ζ as functions of the energy for all *ns* subshells of uranium. The rapid variation of the 6*s* and 7*s* parameters reflects the Cooper minima which occur in these cases.

Upon comparing Figs. 9 and 10, along with Fig. 11, we see that we may roughly classify the curves of each C_{ij} into two categories: those for which the $E1$ contribution is dominant and those for which the contribution from higher multipoles is significant. Naturally, the first group corresponds to the low photon energy cases, i.e., low binding energies (outer shells with $n \gtrsim 5$) and low photoelectron energies ($\lesssim 1$ keV). This group can be extended to $n \geq 2$ shells and $\varepsilon \lesssim 10$ keV, for angles not too close to $\theta=0$ and π (see Fig. 11). Let us call these low-energy outer-shell cases (LEOS's).

We now discuss behavior of the C_{ij} for LEOS at some special angles and energies. Since the behavior of the dipole matrix elements will determine the character of the C_{ij} in LEOS's, we refer to Fig. 6 of Ref. [2] to help understand them. In this figure the radial dipole matrix elements R_1 and R_3 are shown as functions of ε for $ns \rightarrow \varepsilon p_j$, $j=\frac{1}{2}$ and $\frac{3}{2}$, respectively. We note that

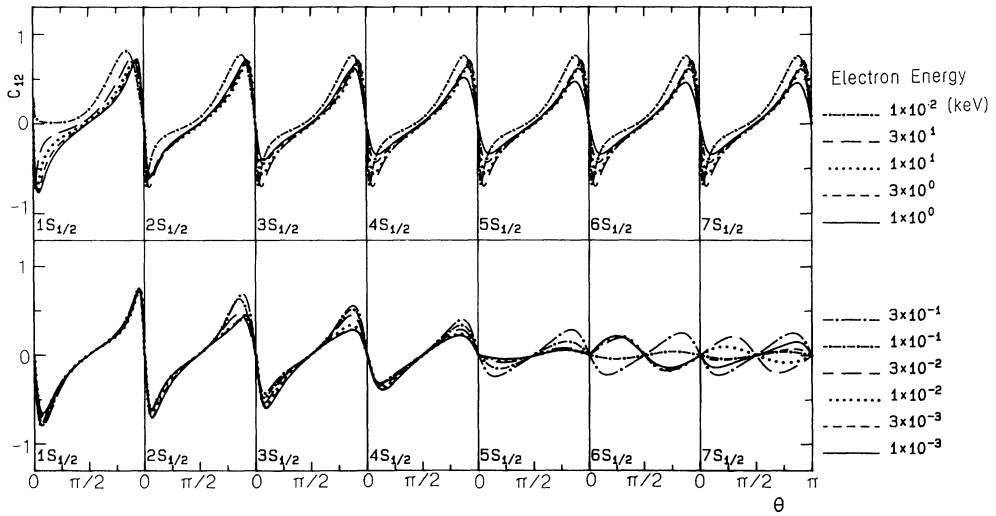

FIG. 4. The same as Fig. 2 for C_{12}.

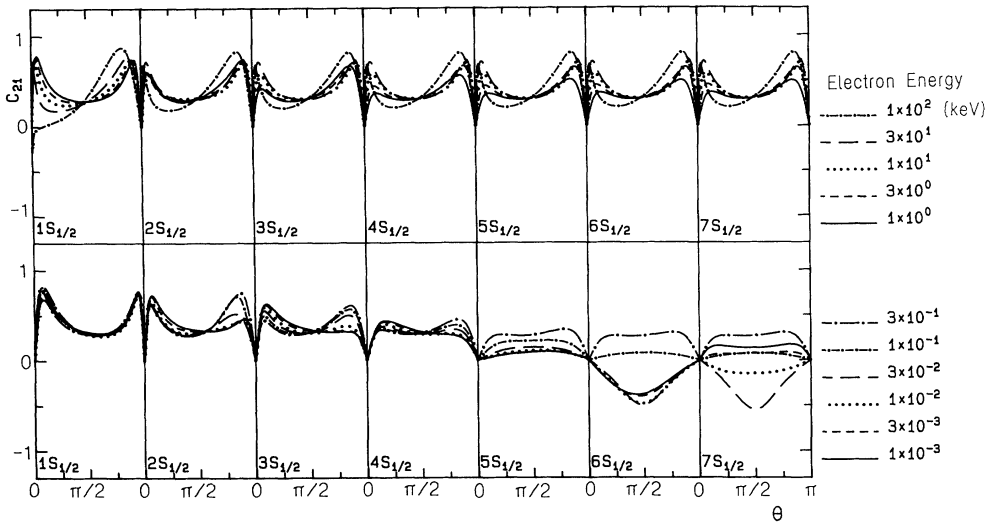

FIG. 5. The same as Fig. 2 for C_{21}.

$R(7s \rightarrow \varepsilon p_{1/2}) \equiv R_1(7s)$ vanishes and changes sign at $\varepsilon \simeq 0.005$ keV, $R_3(6s)$ and $R_3(7s)$ at around $\varepsilon \simeq 0.09$ keV, and that $R_3(5s)$ seems to have a zero just below threshold, with $R_1(5s)$ dominating over $R_3(5s)$ by a factor of more than 3 above threshold up to $\varepsilon \sim 0.1$ keV. When $R_3 = 0$, dipole predictions are as follows: $\beta = 0$ so that the small number of photoelectrons come out independent of the angle θ; C_{10}, C_{21}, and $C_{12} = C_{02}$ become zero independent of θ; and C_{31} and C_{33} become exactly $\sin\theta$ and $\cos\theta$, respectively. There is another case in which the photoelectron angular distribution becomes isotropic for unpolarized photons in the $E1$ limit; namely, when $R_3 + 2R_1 \cos\delta = 0$. At an energy for which this relation is satisfied, C_{10} goes through zero and C_{33} becomes exactly $\cos\theta$. This occurs only for $7s$, at $\varepsilon \sim 0.015$ keV, in between the two low-ε Cooper minima (CM) of $7s$ above threshold. Abrupt changes in the shapes of the C_{ij} curves for LEOS's are clearly understood from these CM and the large separation in energy between CM in R_1 and R_3, resulting in a wide range of energy in which the two radial dipole matrix elements R_1 and R_3 have opposite signs. In the NR limit, these two R's are identical and $\delta = 0$, so that all the C_{ij} vanish except $C_{10} = 1$, which means no spin polarization of the photoelectrons. This aspect of vanishing spin polarization is not a general feature of the NR reduction. It does not occur when there are states of different J in the nonrelativistic subshell and one identifies from which J emission has occurred. It occurs here because only one J can be associated with ns states. As we will see in our subsequent work, for $L > 0$ states spin correlations persist until we sum over $J = L - \frac{1}{2}$ and $J = L + \frac{1}{2}$ initial substates, even if we

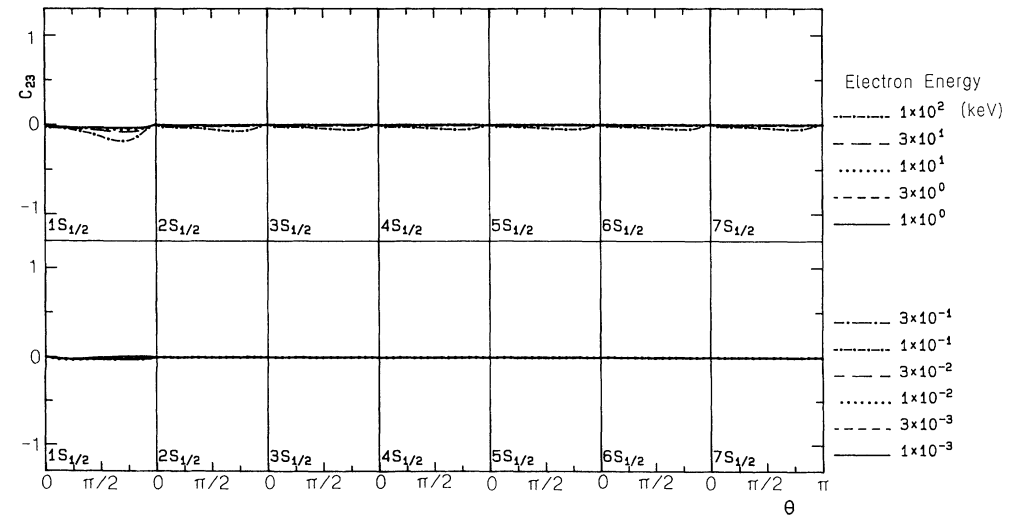

FIG. 6. The same as Fig. 2 for C_{23}.

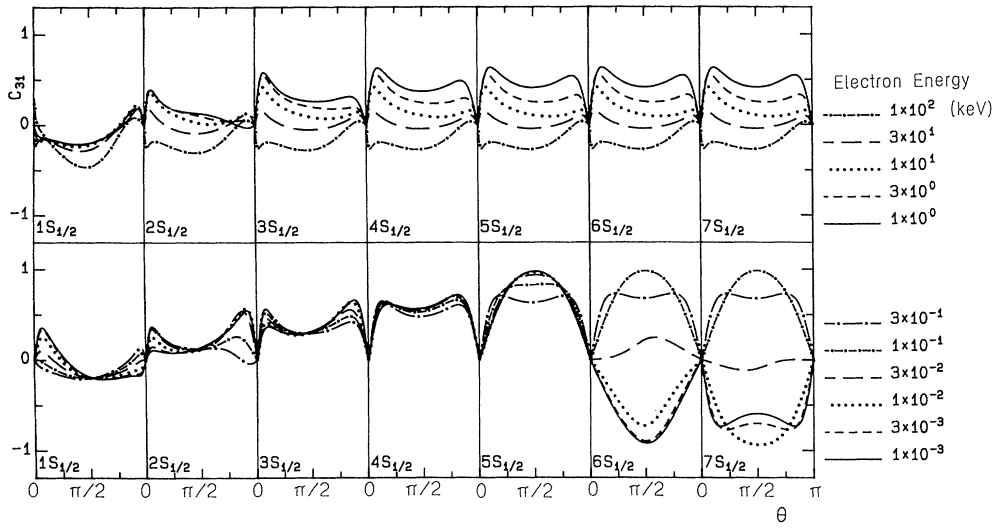

FIG. 7. The same as Fig. 2 for C_{31}.

ignore the difference in energy and wave functions induced from the spin-orbit interaction. This behavior has been mentioned by several authors [6,8,13] and is based on more fundamental features of quantum mechanics.

The spin polarization of photoelectrons from unpolarized photons must be in the direction perpendicular to the production plane, corresponding to the nonvanishing C_{02} shown in Figs. 2, 9(a), and 10(a). C_{12} becomes the same as C_{02} for LEOS's, and we see that the corresponding curves of Figs. 2 and 4 are almost identical. According to Eqs. (15), (16), and (18), these correlation curves cross zero at $\theta=0$, $\pi/2$, and π for all energies of LEOS's, and vanish at all angles with a change in sign when $R_1=0$ or $R_3=0$. The abrupt changes in shape for not only these two but all C_{ij} of 7*s* and 6*s* subshells at low energies up to 0.1 keV are faithfully reproduced in the dipole predictions as shown in Fig. 10.

C_{10} becomes zero at $\theta=0$ and π. According to Eqs. (15), (17), and (23), when $\beta=2$ (or 0) for LEOS's, $C_{10}=1$ (or 0) independent of the angle θ. From Fig. 12 we see that β is close to 2 for $n\leq 3$ for all energies studied, and for $n>3$ for $\varepsilon\gtrsim 1$ keV. In these cases, C_{10} is close to 1 and shows a weak angular dependence away from its zeros at $\theta=0$ and π. For general β $(-1<\beta<2)$ $C_{10}(\theta)$ changes smoothly and reaches an extremum value of $3\beta/(4+\beta)$ at $\theta=\pi/2$ [see Figs 3, 9(a), and 10(a)].

$C_{21}=-C_{02}/\cos\theta$ from Eqs. (16) and (19) for LEOS's; it is zero at $\theta=0$ and π, small at $\theta=\pi/2$. For the cases in which β is close to 2, D_{00} [Eq. (15)] is small at small forward and backward angles. At these angles C_{02} and C_{12} show large values, except when they become identically zero when $R_1=0$ or $R_3=0$, as shown in Figs. 5,

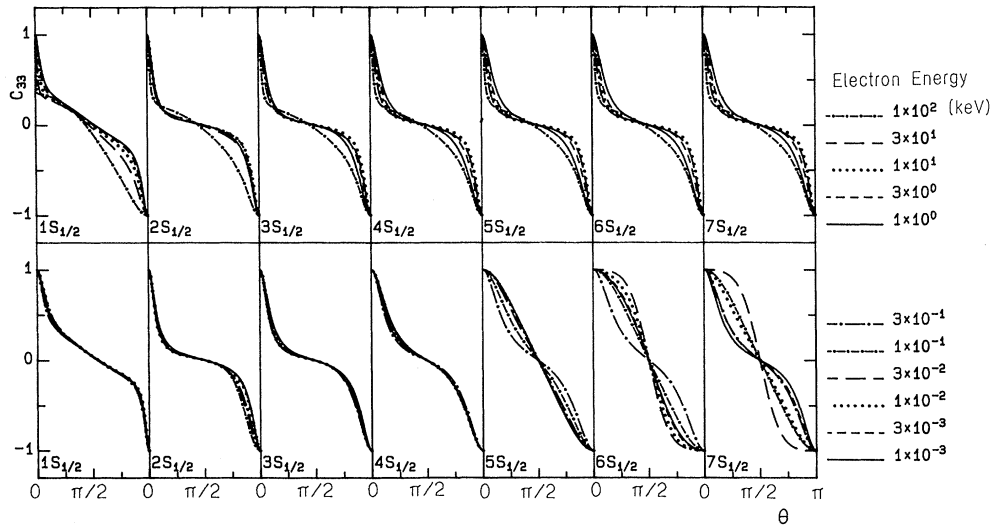

FIG. 8. The same as Fig. 2 for C_{33}.

9(b), and 10(b).

C_{23} in Fig. 6 is seen to be small and in the dipole limit no longitudinal spin polarization is produced from linearly polarized photons. From circularly polarized photons, photoelectrons can be produced polarized either longitudinally or transversely in the production plane, characterized by C_{33} and C_{31}, respectively. C_{31} also vanishes at $\theta=0$ and π, and for LEOS's it reduces to $\sin\theta$ when $\beta=0$, as we see in Figs. 7, 9(b), and 10(b), and from Eqs. (15) and (21). C_{33}, which vanishes at $\theta=\pi/2$, or at all angles for $\beta\equiv 2$, is the only correlation which is nonzero, and, in fact, ± 1 at $\theta=0$ or π, respectively, as in Figs. 8, 9(c), and 10(c), though in LEOS's no photoelectrons come out at exact forward and backward directions. At these

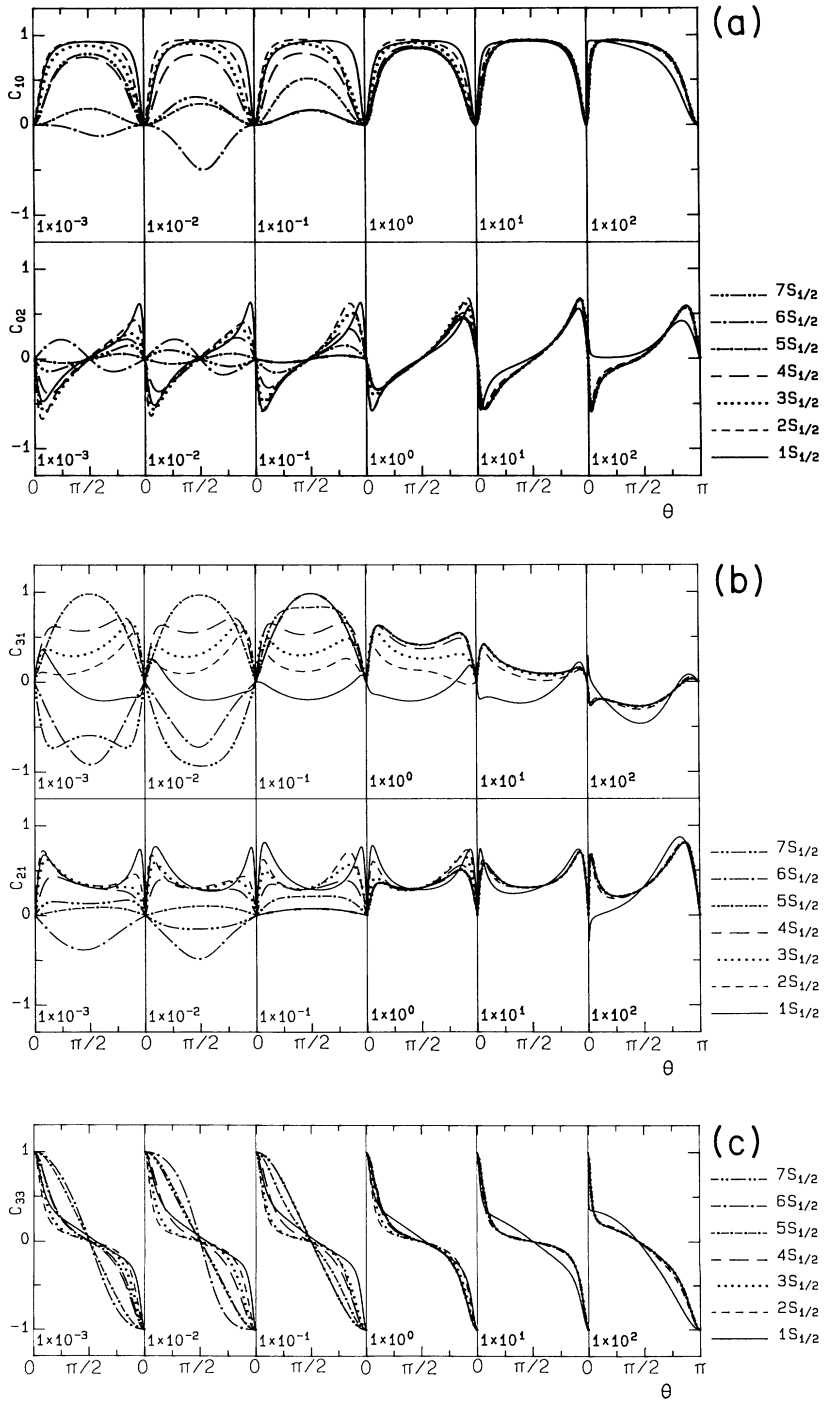

FIG. 9. The same as Fig. 2, but each panel is C_{ij} for a given energy and different n.

angles full correlation follows because the angular momentum transfer is along the initial direction. For LEOS's C_{33} becomes $\cos\theta$ when $\beta=0$.

Dipole predictions begin to fail as the photon energy increases. The contributions from higher multipoles become more pronounced, and the C_{ij} become complicated functions of θ, losing symmetry around $\theta=\pi/2$, just as D_{00} or $d\sigma/d\Omega$ shows forward peaking at high energies. As can be seen from Fig. 11, the deviations from the dipole results are mainly near forward and backward angles. As the energy increases, the range of angle widens and the deviations increase. (Remember that the angular distribution is peaking at the near forward angles.) Also, at high photon energies, curves of any given C_{ij} for all ns subshells show the tendency to merge into a common curve, though the shape of the curve as a function of θ keeps changing with energy as even higher multipoles contribute with increasing photon energies. Curves for $1s$

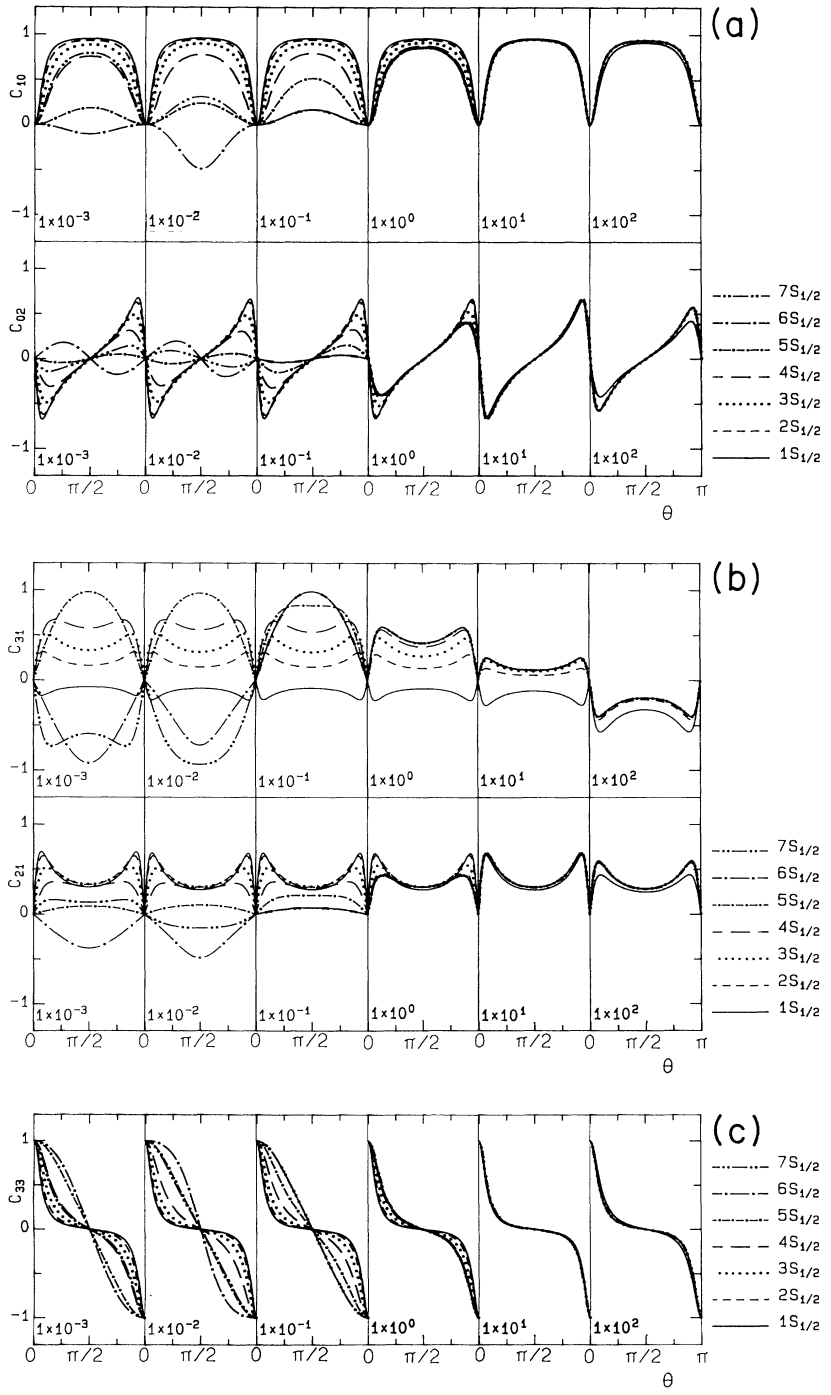

FIG. 10. The dipole predictions of C_{ij} in the same arrangement as in Fig. 9.

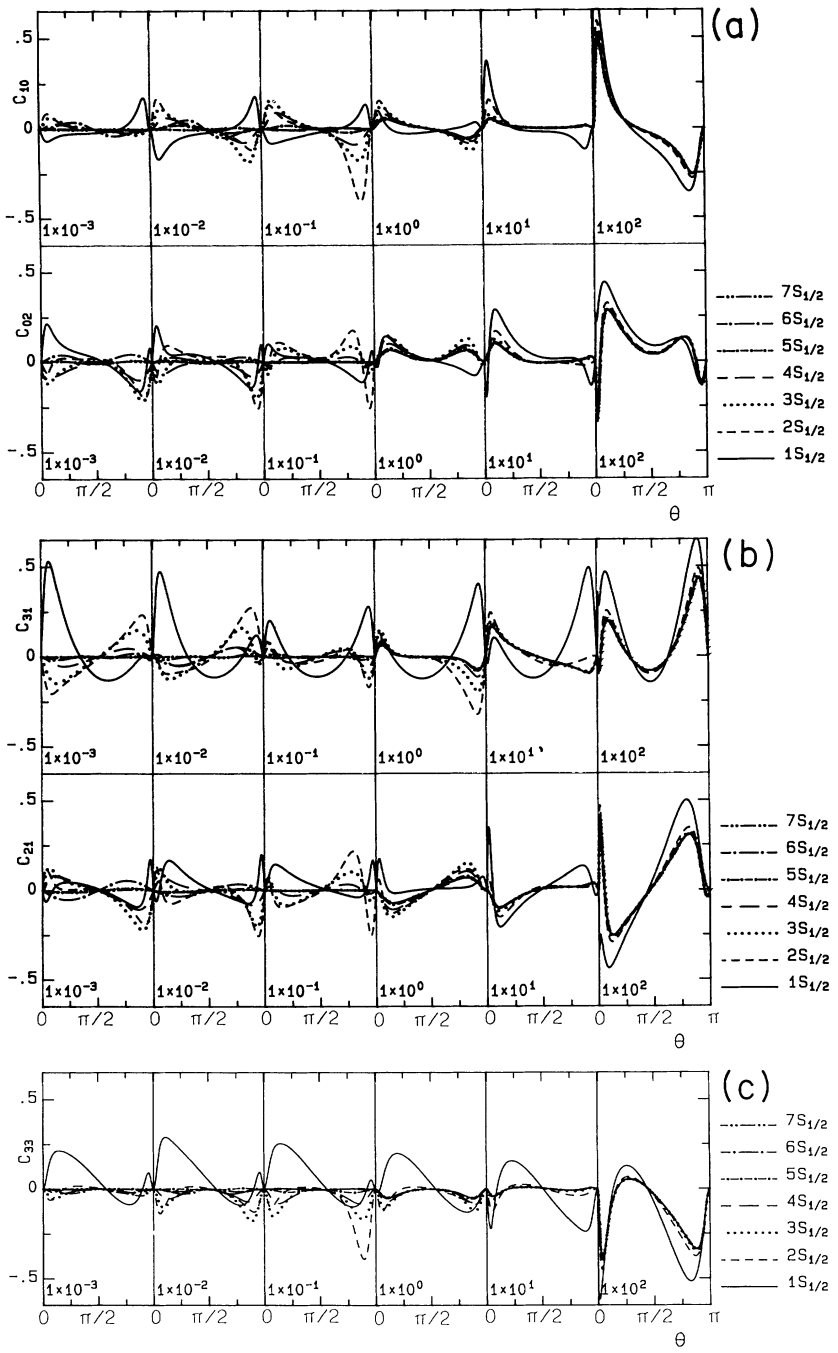

FIG. 11. The differences between the dipole predictions of C_{ij} and the full multipole results.

join the common curve last of all, and the curves for 6*s* and 7*s* as well as the dipole parameters stay together down to ~100 eV, as we see in Figs. 9, 10, and 12. The reason for this merging is the same as discussed before for the angular distributions: At high energies the radial dipole matrix elements are determined in short distance regions of configuration space where the shapes of the wave functions are more or less the same apart from the normalizations. The shape of the 1*s* wave function shows the earliest departure from the common shape. High-energy behavior of C_{ij} is discussed in more detail in Ref. [3].

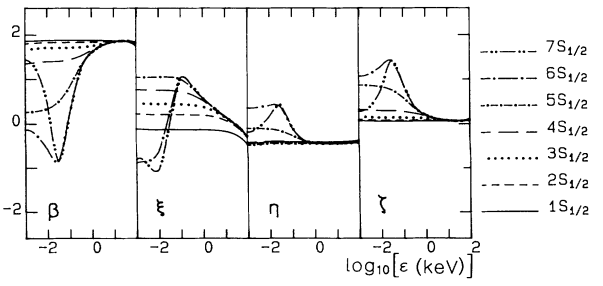

FIG. 12. The dipole parameters β, ξ, η and ζ as functions of the photoelectron energy.

In conclusion, we have studied the photon and photoelectron spin polarization correlations from the *ns* subshells of uranium. LEOS cases are fully reproduced and understood within the dipole formalism; they are very sensitive to the positions of CM. At high energies, the correlations are complicated functions of θ and show the tendency to become independent of n. In subsequent papers of this series we plan to report our results for the polarization correlations of the higher-angular-momentum states of uranium.

ACKNOWLEDGMENTS

This work was supported by NSF Grant No. PHY 90-05763. One of the authors (Y.S.K.) acknowledges support from the Korean Science and Engineering Foundation and wishes to express thanks for the hospitality given by the Center for Theoretical Physics, Seoul National University, where this manuscript was completed.

[1] R. H. Pratt, Akiva Ron, and H. K. Tseng, Rev. Mod. Phys. **45**, 273 (1973).
[2] Y. S. Kim, R. H. Pratt, A. Ron, and H. K. Tseng, Phys. Rev. A **22**, 567 (1980).
[3] R. H. Pratt, R. D. Levee, R. L. Pexton, and W. Aron, Phys. Rev. **134**, A916 (1964).
[4] Akiva Ron, R. H. Pratt, and H. K. Tseng, Chem. Phys. Lett. **47**, 377 (1977).
[5] H. K. Tseng, R. H. Pratt, Simon Yu, and Akiva Ron, Phys. Rev. A **17**, 1061 (1978).
[6] See for example, J. Kessler, in *Polarized Electrons,* 2nd ed., edited by G. Ecker, P. Lambropoulos, and H. Walther, Springer Series on Atoms and Plasmas Vol. 1 (Springer, Berlin, 1985), and references therein.
[7] U. Fano, Phys. Rev. **178**, 131 (1969); **184**, 250 (1969).
[8] N. A. Cherepkov, Zh. Eksp. Teor. Fiz. **65**, 933 (1973) [Sov. Phys.—JETP **38**, 463 (1974)]; J. Phys. B **12**, 1279 (1979).
[9] C. M. Lee, Phys. Rev. A **10**, 1598 (1974).
[10] H. Klar, J. Phys. B **13**, 3117 (1980).
[11] K. N. Huang, Phys. Rev. A **22**, 223 (1980); K. N. Huang, W. R. Johnson, and K. T. Cheng, Atom. Data Nucl. Data Tables **26**, 33 (1981).
[12] J. H. Scofield, Phys. Rev. A **40**, 3054 (1989). The corresponding magnetic multipole $R^{M\Lambda}=(\kappa+K)\int dr(fG+gF)j_\Lambda(kr)$.
[13] U. Heinzman, Appl. Opt. **19**, 4087 (1980).
[14] (η_3,η_1,η_2) in Ref. [6] corresponds to our (ξ_1,ξ_2,ξ_3).
[15] See, for example, G. R. Fowles, *Introduction to Modern Optics,* 2nd ed. (Winstons, New York, 1975), Chap. 2.
[16] An expression for β in the case of a general bound state was given by T. E. H. Walker and J. T. Wabet, J. Phys. B **6**, 1165 (1973).